Journal of Oral Biology and Craniofacial Research 15 (2025) 234–239

Contents lists available at ScienceDirect

Journal of Oral Biology and Craniofacial Research

journal homepage: www.elsevier.com/locate/jobcr

Characterization of upper airway airflow dynamics in young adults with isolated Robin sequence: An exploratory investigation

Maria Noel Marzano-Rodrigues [a], Sergio Henrique Kiemle Trindade [b], Ivy Kiemle Trindade-Suedam [c,*]

[a] School of Medicine, Life and Health Science Institute, Catholic University of Pelotas, Pelotas, Brazil
[b] Laboratory of Physiology, Hospital for Rehabilitation of Craniofacial Anomalies, University of São Paulo and Bauru School of Medicine, University of São Paulo, Brazil
[c] Laboratory of Physiology, Hospital for Rehabilitation of Craniofacial Anomalies, University of São Paulo and Bauru School of Dentistry, University of São Paulo, Brazil

ARTICLE INFO

Keywords:
Robin sequence
Airway obstruction
3D imaging
Fluid dynamics

ABSTRACT

Impaired upper airway dimension in adults with Isolated Robin Sequence (IRS) can alter airflow dynamics, increasing the risk of pharyngeal collapse and the onset of obstructive sleep apnea. This study aimed to characterize the upper airways of six young adults (20.83 ± 6.40 years) with IRS, using computational fluid dynamics. Upper airways of six patients were reconstructed using 3D segmentation, generating unstructured hybrid meshes with ≥4 million tetrahedral elements. Flow simulations at 15 l/min were solved using the realizable k-ε model and the finite volume method. Morphophysiological variables assessed were: total airway volumes, minimal cross-sectional areas, average pressure, velocity magnitude, wall shear stress, turbulent kinetic energy (k) production, and resistance. Airway volume corresponded to 29.32 ± 4.65 cm^3 and minimal cross-sectional area was 1.00 ± 0.55 cm^2. Pressure drop, airway resistance to airflow, velocity of the airflow and turbulent kinetic energy corresponded to 31.341 ± 15.837 Pa, 0.125 ± 0.063 (Pa s/ml), 1.882 ± 0.514 (m/s) and 0.152 ± 0.056 (m2/s2). The total airway volume exhibited a strong negative correlation with airway resistance (−0.899) and the inlet-to-outlet pressure drop (−0.899). The minimal cross-sectional area of the pharynx at the retroglossal level showed a strong negative correlation (−0.912) with the area-weighted average velocity magnitude of the airflow and with k production (−0.924). In conclusion, airway volume reduction and retroglossal obstruction in young adults with IRS are associated with altered fluid flow characteristics, including increased velocity magnitude, pressure drop, resistance, and turbulent kinetic energy production. These changes may increase the effort to breathe and predispose patients to sleep-disordered breathing.

1. Introduction

Isolated Robin Sequence (IRS), with an incidence rate ranging from 1 per 8500 to 1 per 14,000 births, is characterized by micrognathia, glossoptosis, and respiratory obstruction, with variable involvement of cleft palate.[1–3] It presents a heterogeneous clinical spectrum, resulting in varying degrees of stomatognathic dysfunction and upper airway impairment.[4,5]

Theoretically, the spontaneous resolution of airway obstruction in IRS, primarily attributed to tongue-based mechanisms,[6] relies on the concept of mandibular "catch-up" growth.[7–9] However, nearly 40 % of these patients require orthognathic surgery upon reaching skeletal maturity.[10] Consequently, in conservatively treated patients with persistent retrognathia, glossoptosis and pharyngeal obstruction are likely to persist into adulthood. Furthermore, the presence of a cleft palate exacerbates the risk of airway obstruction.[11,12] As a result of multisite upper airway constrictions, obstructive sleep apnea (OSA) may develop[12–14] and is often linked to cardiometabolic complications and high morbidity,[15] making it a critical concern in the long-term management of patients with craniofacial anomalies.

The combination of cone-beam computed tomography (CBCT) and three-dimensional (3D) segmentation of the upper airway in patients with craniofacial anomalies is a reliable assessment method for identifying unfavorable anatomical characteristics associated with reduced airway patency and obstructive events.[14,16–18] However, this method does not provide airflow dynamic characterization,[19] which can be

* Corresponding author. Rua Silvio Marchione 3-20, Laboratório de Fisiologia - Hospital for Rehabilitation of Craniofacial Anomalies, University of São Paulo, SP, CEP 17102-900, Bauru, Brazil.
E-mail address: ivytrin@usp.br (I.K. Trindade-Suedam).

https://doi.org/10.1016/j.jobcr.2025.01.009
Received 17 December 2024; Received in revised form 7 January 2025; Accepted 8 January 2025
Available online 10 February 2025

clinically assessed through peak nasal inspiratory flow and rhinomanometry.[20–24] Recently, computational fluid dynamics (CFD) has emerged as a novel technology for analyzing airflow behavior, with preliminary data showing good correlations with rhinomanometry[25] and patient-reported symptoms.[26,27]

Patients with IRS could particularly benefit from CFD simulations due to the high prevalence of morphofunctional imbalances and airway obstructions, as well as the frequent need for surgical interventions. Therefore, this study aimed to characterize the upper airways of six patients with IRS by analyzing area-weighted average pressure, velocity magnitude, wall shear stress, turbulent kinetic energy production, and resistance using CFD simulations. It is our hypothesis that young adults with IRS will exhibit a reduction in the volume of the upper airway and minimal cross-sectional area especially those located in the oropharynx. Furthermore, it is expect to observe an association between these parameters and the occurrence of negative pressures, as well as greater resistance to airflow, which may predispose individuals to sleep disorders.

2. Methods

2.1. Ethical considerations, study design, and settings

The study protocol was approved by the Institutional Review Board (process number - CEP/CONEP (CAAE): 15205413.7.0000.5441) and complied with the World Medical Association Declaration of Helsinki. This retrospective case series was developed at a tertiary hospital for the rehabilitation of craniofacial anomalies (Hospital for Rehabilitation of Craniofacial Anomalies, University of São Paulo, Bauru, São Paulo, Brazil).

2.2. Sample selection and cone-beam computed tomography

A database of 672 imaging exams of individuals with IRS was screened. Exclusion criteria encompassed: individuals younger than 15 years, those with chronic upper airway infections, hypertrophic tonsils or adenoids, a history of orthognathic surgery, or proliferative/destructive lesions in soft or hard tissues.[18] The CBCT scans included in the study were originally obtained for medical or dental purposes, all with a full field of view (FOV). Images were acquired with patients in a seated position using the i-CAT Next Generation scanner (ISI-i-CAT Imaging Sciences International, Hatfield, PA, USA). The acquisition parameters were as follows: 16 × 13 cm field of view, 26.9-s exposure time, 120 kV, 37 mA, 0.25 mm voxel resolution, and 0.25 mm slice thickness.[16] After applying the exclusion criteria, six scans were selected for analysis.

2.3. 3D evaluation and CFD simulation

2.3.1. Preprocessing

The upper airway, encompassing the nasal cavity and pharynx, was the domain of interest, while the paranasal sinuses were excluded from the airway segmentation.[14,17] The CBCT images, stored in Digital Imaging and Communications in Medicine (DICOM) format, were imported into the open-access image analysis algorithm ITK-SNAP 3.8.0 (2019, http://www.itksnap.org) for 3D active contour segmentation.[28] The selected threshold ranged from −1000 to −550 Hounsfield units, which minimized the need for manual artifact correction.[24]

The anterior boundary of the airway corresponded to the external nostrils while the inferior boundary corresponded to the epiglottis valve and total airway volume was automatically calculated (mm^3). Minimal CAD cleaning was performed using Ansys 2020.R2 SpaceClaim (Ansys, Inc., Pennsylvania, USA) to preserve the anatomical characteristics of the patient's upper airway. Regarding minimal area assessment, the following parameters were considered for analysis: CSA1 refers to the nasal valve, CSA2 to the anterior region of the inferior and medial conchae, CSA3 to the posterior region of the inferior and medial conchae, CSA4 to the cranial limit of the nasopharynx, CSA5 to the cranial limit of the oropharynx, and CSA6 to the pharyngeal minimal cross-sectional area (retroglossal) (Fig. 1).

The geometry, created in ANSYS 2020.R2 SpaceClaim (Ansys Inc.), consisted solely of fluid regions with no voids. Therefore, the Watertight Geometry workflow in ANSYS 2020.R2 Fluent, along with Fluent Meshing (Ansys Inc.), was used for mesh generation. Unstructured hybrid meshes with over 4 million elements, including tetrahedral elements and three layers of prisms that grow only on the walls, were provided.[29] The mesh quality was verified using inverse orthogonal quality (OQ) and aspect ratio (AR) criteria.

2.3.2. Solver

Adiabatic, turbulent flows were simulated using ANSYS Fluent 2020. R2 (Ansys Inc.). The fluid properties were set to constant density (1.225 kg/m^3) and constant viscosity (1.7894E-05 kg/m·s). Boundary conditions included inlets (right and left nostrils) with a gauge pressure of 0 Pa, an outlet (at the CIV level) with a mass flow rate of 0.00031 kg/s (15 L/min), and no-slip stationary walls with standard roughness. The realizable k-ε model was used to solve bidirectional flow simulations in the discretized geometries through the finite volume method. Hybrid method initialization with constant pressure was applied, and calculations were performed with a time scale factor of 1 and 200 iterations.

In the transport equations: G_k = represents the generation of turbulence kinetic energy due to mean velocity gradients; G_b is the turbulence kinetic energy due to buoyancy; Y_M = is the contribution of fluctuating dilatation in compressible turbulence to the overall dissipation rate; C_2 is a constant (1.9); $C_{1\epsilon}$ is a constant (1.44); σ_k is the turbulent Prandtl number for k (1.0); σ_ϵ = is the turbulent Prandtl number for ϵ (1.2); S_k and S_ϵ are user-defined source terms.

$$\frac{\partial}{\partial t}(\rho k)+\frac{\partial}{\partial x_j}(\rho k u_j)=\frac{\partial}{\partial x_j}\left[\left(\mu+\frac{\mu_t}{\sigma_k}\right)\frac{\partial k}{\partial x_j}\right]+G_k+G_b-\rho\epsilon-Y_M+S_k$$

$$\frac{\partial}{\partial t}(\rho\epsilon)+\frac{\partial}{\partial x_j}(\rho\epsilon u_j)=\frac{\partial}{\partial x_j}\left[\left(\mu+\frac{\mu_t}{\sigma_\epsilon}\right)\frac{\partial \epsilon}{\partial x_j}\right]+\rho C_1 S\epsilon-\rho C_2\frac{\epsilon^2}{k+\sqrt{\nu\epsilon}}+C_{1\epsilon}\frac{\epsilon}{k}C_{3\epsilon}G_b+S_\epsilon$$

In the eddy viscosity equation, C_μ is not a constant, but a function of the mean strain and rotation rates, the angular velocity of the system rotation, and the turbulence fields in k and ϵ:

$$\mu_t=\rho C_\mu\frac{k^2}{\epsilon}$$

Reynolds (Re) numbers were calculated for each case, according to the equation:

$$Re=\frac{pVD}{\mu}$$

were p = fluid density (1.225 kg/m^3), V = fluid velocity (m/s), D = mean nasal valve diameter (m), μ = fluid dynamic viscosity (1.7894 E^{-05} kg/m-s).

The convergence of each simulation was assessed using the following criteria: 1) residual error values $< 10^{-3}$; 2) steady solution of the area-weighted average for the monitoring point at the outlet; and 3) domain imbalance <1 %. Considering the similarity of the geometries and meshes used in this study with those assessed by Frank-Ito et al.,[29] no mesh independency tests were performed. According to the authors, ≥4 million element grids produced results with negligibly small variations between the sinonasal airflow and particle transport simulations.[29]

2.3.3. Postprocessing

Simulations were assessed by quantitative (mass flow report balance and surface integrals) and qualitative means (contours). The area-

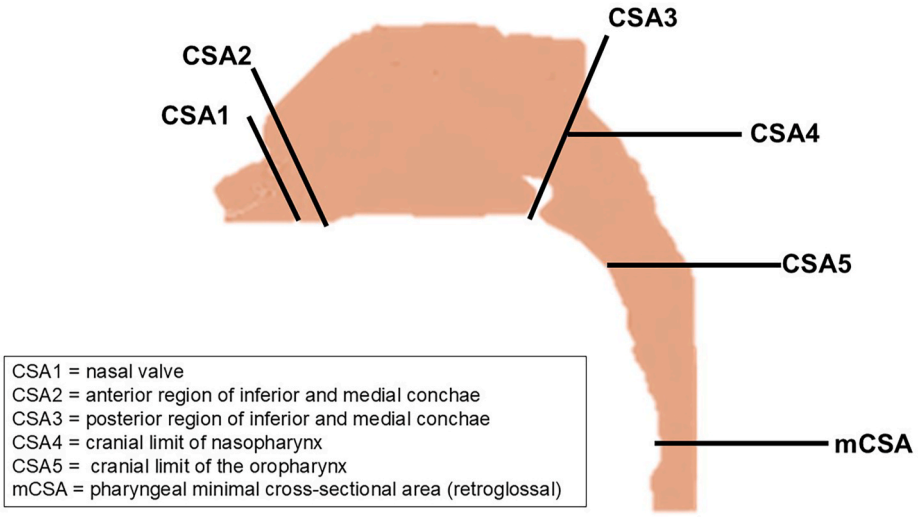

Fig. 1. Anatomical locations of minimal cross-sectional areas (CSA) in the upper airways.

weighted average pressure, velocity, wall shear stress, volume mass flow and production of turbulent kinetic energy (k) were extracted. The area-averaged pressure drop (ΔP) from inlet to the outlet (total airway), from inlet to choana (nasal cavity) and from choana to outlet (pharynx) were defined to verify the effect of the airway narrowing on airflow behavior. Resistance of the airways were calculated using the following equation:

$$R = \frac{\Delta P}{Q}$$

where, R = resistance (Pa.s/ml) and Q = volume flow rate (ml/s).

Sample characteristics were given as mean ± standard deviation (SD) and Pearson's correlation coefficient (Pearson's r) was used for evaluating the correlation between fluid flow characteristics with airway dimensions. $P \leq 0.05$ was considered to be statistically significant.

3. Results

The upper airways of six young adults with IRS (20.83 ± 6.40 years), including four females and two males, were evaluated. Table 1 presents the demographic data and the average airway dimensions in young adults with isolated Robin sequence. The total airway volume was 29.32 ± 4.65 cm^3 while the minimal cross-sectional area (mCSA) corresponded to 1.00 ± 0.55 cm^2. Considering the diameters of the nasal valve (mean 11.87 ± 0.93 mm) and the minimal cross-sectional area (mCSA) for each case, the Reynolds numbers ranged from 1668.60 ± 150.80 at the nasal valve to 2875 ± 765.83 at the mCSA, indicating transitional fluid airflow. This indicates that the airflow in these regions is neither fully laminar nor fully turbulent but may fluctuate between these two types depending on local conditions.

Table 2 summarizes the area-weighted average ΔP (Pa), velocity magnitude (m/s), turbulence kinetic energy production (k) (m^2/s^2), and the resistance (R) values for the total airway, anatomical airway segments, and mCSA. Turbulence intensity ranged from 5.93 % to 52.88 %, with the highest mean values observed at the nasal valve (38.52 ± 8.87 %) and at the mCSA (31.66 ± 13.62 %). The mean wall shear stress value was 0.25 ± 0.31 Pa, with a minimum of 0.06 Pa and a maximum of 0.89 Pa.

The total airway volume exhibited a strong negative correlation with airway resistance (R) (−0.899) (0.12 ± 0.06 Pa s/mL) and the inlet-to-outlet area-weighted average static ΔP (−0.899) (31.34 ± 15.83 Pa). The pharyngeal mCSA at the retroglossal level (1.00 ± 0.55 cm^2) showed a strong negative correlation (−0.912) with the area-weighted average velocity magnitude of the airflow (3.47 ± 2.05 m/s) and with turbulence kinetic energy production (−0.924) (0.20 ± 0.17 m^2/s^2). No other statistically significant correlations were detected. The contours of velocity magnitude, vectors, pressure, and wall shear stress for two cases are shown in Fig. 2 for illustrative purposes.

Table 1
Characterization of airway dimensions in young adults with isolated Robin sequence (sample size = 6).

Case	Demographics		Airway dimensions							
			Total volume (cm^3)	Cross sectional areas (CSA) (cm^2)						
	Sex	Age		mean inlet	CSA1	CSA2	CSA3	CSA4	CSA5	mCSA	outlet
1	♀	15	25.84	0.34	1.47	1.86	2.00	4.02	2.35	0.80	1.12
2	♀	17	30.95	0.67	1.55	1.36	3.47	4.63	1.99	1.35	3.20
3	♀	18	34.12	0.65	1.20	1.92	2.00	5.53	4.23	1.87	2.98
4	♀	29	24.10	0.41	1.26	1.95	1.90	2.02	1.59	0.45	3.54
5	♂	17	25.94	0.65	1.36	2.95	1.65	4.22	2.76	0.44	0.53
6	♂	29	34.98	0.57	1.22	3.96	5.90	5.30	2.58	1.09	1.15
$\underline{X}$ ±SD		**20.83 ± 6.40**	**29.32 ± 4.65**	**0.55 ± 0.14**	**1.34 ± 0.14**	**2.33 ± 0.14**	**2.82 ± 0.94**	**4.29 ± 1.25**	**2.59 ± 0.91**	**1.00 ± 0.55**	**2.15 ± 1.25**

Abbreviations: $\underline{X}$ = mean, SD = standard deviation, age (years),♀ = female, ♂ = male, CSA1 = nasal valve, CSA2 = anterior region of inferior and medial conchae, CSA3 = posterior region of inferior and medial conchae, CSA4 = cranial limit of nasopharynx, CSA5 = cranial limit of the oropharynx, mCSA = pharyngeal minimal cross-sectional area (retroglossal).

Table 2
Given absolute values of CFD quantitative variables for the assessment of airflow in young adults with isolated Robin sequence (sample size = 6).

Airway segment	Fluid flow characteristics							
	ΔP (Pa)		R (Pa.s/ml)		Velocity (m/s)		k (m^2/s^2)	
	$\underline{X}$ ±SD	Min-Max	$\underline{X}$ ±SD	Min-Max	$\underline{X}$ ±SD	Min-Max	$\underline{X}$ ±SD	Min-Max
Total airway	31.341 ± 15.837	12.96–50.33	0.125 ± 0.063	0.051–0.201	1.882 ± 0.514	0.579–6.260	0.152 ± 0.056	0.032–0.490
Nasal cavity	18.639 ± 6.397	8.26–25.01	0.075 ± 0.026	0.064–0.100	1.868 ± 0.805	0.618–4.550	0.126 ± 0.121	0.002–0.490
Pharynx	12.701 ± 13.646	1.49–34.04	0.051 ± 0.055	0.005–0.136	1.896 ± 1.576	0.579–6.260	0.153 ± 0.120	0.031–0.443

Abbreviations: $\underline{X}$ = mean, SD = standard deviation, Min = minimum, Max = maximum, ΔP (Pa) = pressure drop, R (Pa.s/ml) = resistance, k (m^2/s^2) = turbulent kinetic energy.

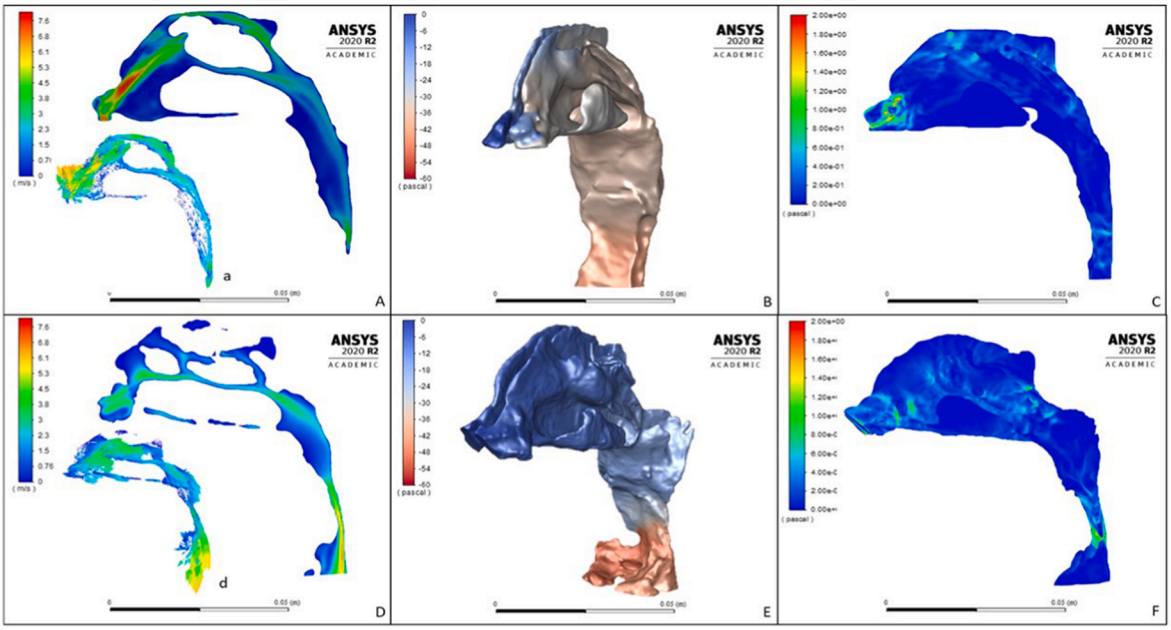

Fig. 2. Airflow contours in YZ axis and airway walls of two young adults with isolated Robin sequence. A and D - showed increased velocity magnitude at the nasal valve (NV) and pharyngeal minimal cross-sectional area (mCSA), with airflow direction changing from vertical for horizontal at the NV, flow separation at the pharynx and turbulence at the mCSA (a and d). B and E – More intense negative pressure gradient at the pharyngeal mCSA. C and F - Increased wall shear stress at NV and mCSA.

4. Discussion

This study evaluated six young adults with IRS, despite efforts to include all regularly registered IRS patients at the Hospital for Rehabilitation of Craniofacial Anomalies, University of São Paulo, Bauru, São Paulo, Brazil. Although the sample is not representative, it offers a rare and potentially unique report on airflow characteristics assessed through CFD in this specific and relatively uncommon population. The focus of this study is to enhance the understanding of airway dynamics in this population, which is of particular interest due to their high risk of sleep apnea, a condition that often begins with skeletal alterations, leading to changes in respiratory flow dynamics and their medium- and long-term systemic consequences. Furthermore, the airway was reconstructed in 3D, providing volumetric dimensions and area measurements at various anatomical points. To date, no previous studies on airway morphometry in adults with IRS allow for direct comparison of results.

In other craniofacial anomalies, such as cleft lip and palate—which is more prevalent (1 in 1000 births)[30] than IRS—the associations between altered craniofacial morphology, reduced upper airway dimensions,[11,14,16,18] and the onset of OSA[12,14] are well documented. In contrast, there is a lack of data regarding the developmental outcomes of skeletal and airway morphology in IRS patients.[4,10]

Yatabe-Ioshida et al.[17] measured airway volumes in adults with unilateral and bilateral cleft palate before and after orthognathic surgery. The preoperative mean values for these groups were 23.23 ± 6.71 cm^3 and 31.58 ± 7.28 cm^3, respectively. Similarly, Campos et al.[14] assessed adults with unilateral and bilateral cleft lip and palate, reporting airway volumes of 43.00 ± 9.00 cm^3 in patients without OSA and 36.00 ± 5.00 cm^3 in those with OSA. The airway volume in young adults with IRS was comparable to that observed in cleft lip and palate patients prior to orthognathic surgery and in those with OSA. Additionally, Campos et al.[14] reported a mean mCSA at the oropharynx level of 0.94 ± 0.19 cm^2 in subjects with cleft lip and palate and OSA. In this anatomical region, the mCSA in individuals with IRS was nearly 50 % smaller, indicating severe obstruction due to glossoptosis, as expected.

A negative correlation was observed between pharyngeal mCSA and airflow velocity magnitude, which can be attributed to the Bernoulli effect in the retroglossal area[16] and the production of k. The mCSA where velocity peaks occur has been proposed as the primary site for obstructive events due to its greater collapsibility, particularly in the retropalatal and oropharyngeal regions.[31,32] Turbulent kinetic energy, which describes the concentration of turbulent flow in the upper airway, is characterized by the root-mean-square velocity fluctuation. At the mCSA, increased flow intensity results in higher velocity and turbulent kinetic energy, a phenomenon likely responsible for obstructive respiratory events in these patients (Faizal et al., 2021).

In clinical respiratory terms, turbulent kinetic energy production refers to the physical phenomenon that occurs when airflow in the airways transitions from laminar (smooth and organized) to turbulent (irregular and chaotic). This concept is significant in respiratory dynamics studies because it directly impacts airflow efficiency and resistance within the airways, often becoming evident in the presence of an obstruction. Consequently, in individuals with IRS, the oropharyngeal region should be thoroughly evaluated for airway obstruction diagnosis and management, considering the presence of glossoptosis, reduced oropharyngeal cross-sectional dimensions, increased flow velocity, and turbulent kinetic energy. Furthermore, the total airway volume in the assessed IRS individuals showed a strong negative correlation with pressure drop and resistance, indicating a clinically significant reduction in airway ventilation and an increased breathing effort.

In these six cases, the highest wall shear stress was observed at the nasal valve and the pharyngeal mCSA. At the nasal valve, the airflow shifts from vertical to horizontal, generating high pressure and stress, which aligns with previous findings (Tan et al., 2012). The increased wall shear stress at the oropharynx tends to bring the anterior and posterior walls of the airway closer together, altering airflow profiles and contributing to airway collapse.[33,34]

Regarding the CFD method, the steady flow rate used in this study (15 l/min, 0.00031 kg/s) represents low physical activity levels[35] and is typically assumed to be laminar in most studies. However, transitioning flows are commonly associated with obstructed airways[36] and OSA, which can occur even during breathing at rest.[37] Furthermore, at a flow rate of 10 l/min,[38,39] transitional phases have been observed due to the structural complexity of the airway, adverse pressure gradients, secondary flow regions, and recirculation zones. Our findings suggest that airflow in the studied airways exhibits unsteady transitional flow even under low Reynolds numbers. This finding has significant clinical implications, as it highlights the potential for increased airflow resistance and turbulence even during low-intensity breathing, which may contribute to the onset or exacerbation of respiratory symptoms in individuals with compromised airway structures.

It is worth noting that the laminar flow model was initially used as a starting point. However, convergence was not achieved for flow rates of 15 l/min. The k-ε model is one of the most commonly used turbulence models in CFD simulations (Stapleton et al., 2003). Nevertheless, its accuracy in predicting airflow[38,40–42] and particle deposition (Stapleton et al., 2003) in the upper airways is debated due to larger dispersion, insufficient responsiveness to streamline curvature, and limitations in handling separated flow.[35,42]

Considering these challenges and the airway characteristics in IRS, including irregular shapes and area variations that promote turbulence, the realizable k-ε model with standard wall functions was selected for CFD simulations. The realizable k-ε model differs from the traditional k-ε model by introducing a new formulation for turbulence viscosity and a new transport equation for the dissipation rate. These features allow it to more accurately predict the spreading rates of both planar and round jets, as well as enhance performance for flows involving rotation, boundary layers under strong adverse pressure gradients, and recirculation.

For instance, Ma and Lutchens[43] successfully utilized the realizable k-ε model to simulate aerosol deposition in the human respiratory system. However, the limitations of turbulence models primarily affect measurements at the subglottic level, where airflow anomalies like round-jet/plane-jet behavior and flow separation are present.[35,42] Therefore, minimal effects are anticipated for simulations in the nasal cavity and pharynx, where these anomalies are less significant.

From a clinical perspective, the use of the realizable k-ε model in CFD simulations offers valuable insights into the complex airflow dynamics in IRS individuals. It allows for a more accurate assessment of areas prone to obstruction, such as the nasal cavity and pharynx, and provides critical data on airflow characteristics that could guide the diagnosis and management of respiratory conditions. This configuration enables the identification of regions with increased turbulence, pressure drops, or flow separation, which are directly relevant for tailoring interventions to improve airway patency and reduce respiratory effort.

Although considerable progress has been made in understanding the flow field inside the upper airway through CFD, the complexity of airflow behavior still requires further clarification through in vitro and in vivo physical validation.[25,35,37,40,41,44] Additionally, future studies that effectively determine whether adults with IRS could benefit from procedures aimed at increasing oropharyngeal dimensions would be highly valuable for managing obstructed airways in this population. Such research could provide crucial insights into the potential benefits of targeted interventions for improving airflow and reducing respiratory complications in these patients.

It is important to recognize that the present study is limited by a small sample size and the absence of a control group, which restricts the ability to draw more robust conclusions. Future studies with larger sample sizes and control groups would be essential to strengthen these findings and provide more conclusive evidence. However, despite these limitations, this study provides a unique description of the respiratory pattern in young adults with IRS, a rare condition, with the purpose of understanding the effects of airway morphology on respiratory physiology.

Finally, the study's aim is to explore and analyze the relationship between skeletal alterations and respiratory dysfunction in this high-risk population. This knowledge has the potential to inform future clinical applications, even if it is in the exploratory phase at this stage. We also acknowledge that the current study is not yet providing direct clinical interventions but is laying the foundation for future research that could have clinical value.

In conclusion, this study is the first attempt to characterize airflow in young adults with IRS. The results reinforce the role of volumetric airway impairment and retroglossal constriction in obstructive events in adults with IRS, demonstrated through the correlation between airway volume and cross-sectional areas with fluid flow characteristics, such as increased velocity magnitude, pressure drop and resistance, and production of turbulent kinetic energy.

Declaration of non-use of identifiable images and patient consent exemption

We hereby declare that this study does not include identifiable images or data that could reveal the identity of individual participants. All data used are anonymized and do not contain any personal or identifiable information.

As such, the requirement for obtaining patient consent is waived, as there is no risk to participant confidentiality or privacy. The study adheres to the relevant ethical guidelines and institutional policies regarding the use of anonymized data.

Ethical approval

The study was approved by the Institutional Review Board at HRAC-USP, under protocol number: CEP/CONEP (CAAE): 15205413.7.0000.5441.

Funding

1. CAPES (Coordination for the Improvement of Higher Education Personnel - CAPES PRODOC 23038.035176/2008-1)
2. FAPESP (The São Paulo Research Foundation - 13501-0/2014) for the financial support.

Declaration of competing interest

The authors declare that they have no known competing financial interests or personal relationships that could have appeared to influence

the work reported in this paper.

Acknowledgments

We would like to thank the volunteers who participated in this research for their invaluable collaboration. We also extend our gratitude to the Graduate Program in Rehabilitation Sciences at HRAC-USP for making this research possible and for their essential support.

References

1. Printzlau A, Andersen M. Pierre Robin sequence in Denmark: a retrospective population-based epidemiological study. *Cleft Palate Craniofac J*. 2004;41:47–52.
2. Maas C, Poets CF. Initial treatment and early weight gain of children with Robin Sequence in Germany: a prospective epidemiological study. *Arch Dis Child Fetal Neonatal Ed*. 2014;99:F491–F494.
3. Motch Perrine SM, Wu M, Holmes G, Bjork BC, Jabs EW, Richtsmeier JT. Phenotypes, developmental basis, and genetics of Pierre Robin complex. *J Dev Biol*. 2020;8:30–51.
4. Laitinen SH, Heliövaara A, Ranta RE. Craniofacial morphology in young adults with the Pierre Robin sequence and isolated cleft palate. *Acta Odontol Scand*. 1997;55:223–228.
5. Logjes RJH, Upton S, Mendelsohn BA, et al. Long-term speech outcomes of cleft palate repair in Robin Sequence versus isolated Cleft Palate. *Plast Reconstr Surg Glob Open*. 2021;9:e3351–e3360.
6. Runyan CM, Uribe-Rivera A, Tork S. Management of airway obstruction in infants with pierre Robin sequence. *Plast Reconstr Surg Glob Open*. 2018;6:e1688–e1695.
7. Figueroa AA, Glupker TJ, Fitz MG, BeGole EA. Mandible, tongue, and airway in Pierre Robin Sequence: a longitudinal cephalometric study. *Cleft Palate Craniofac J*. 1991;28:425–434.
8. Matsuda A, Suda N, Motohashi N, Tsuji M, Ohyama K. Skeletal characteristics and treatment outcome of five patients with Robin sequence. *Angle Orthod*. 2006;76:898–908.
9. Purnell CA, Janes LE, Klosowiak JL, Gosain AK. Mandibular catch-up growth in Pierre Robin Sequence: A systematic review. *Cleft Palate Craniofac J*. 2019;56:168–176.
10. Pfaff MJ, De Leon F, Le L, et al. Long-term orthognathic considerations in the pierre Robin sequence patient. *Plast Reconstr Surg*. 2020;146:599e–606e, 349.
11. Fukushiro AP, Trindade IE. Nasal airway dimensions of adults with cleft lip and palate: differences among cleft types. *Cleft Palate Craniofac J*. 2005;42:396–402.
12. Cielo CM, Taylor JA, Vossough A, et al. Evolution of obstructive sleep apnea in infants with cleft palate and micrognathia. *J Clin Sleep Med*. 2016;12:979–987.
13. Robison JG, Otteson TD. Increased prevalence of obstructive sleep apnea in patients with cleft palate. *Arch Otolaryngol Head Neck Surg*. 2011;137:269–274.
14. Campos LD, Trindade IEK, Yatabe M, et al. Reduced pharyngeal dimensions and obstructive sleep apnea in adults with cleft lip/palate and Class III malocclusion. *Cranio*. 2019;17:1–7.
15. Drager LF, Santos RB, Silva WA, et al. OSA, Short sleep duration, and their interactions with sleepiness and cardiometabolic risk factors in adults: The ELSA-Brasil study. *Chest*. 2019;155:1190–1198.
16. Trindade-Suedam IK, Lima TF, Campos LD, Yaedú RYF, Filho HN, Trindade IEK. Tomographic pharyngeal dimensions in individuals with unilateral cleft lip/palate and Class III malocclusion are reduced when compared with controls. *Cleft Palate Craniofac J*. 2017;54:502–508.
17. Yatabe-Ioshida MS, Campos LD, Yaedu RY, Trindade-Suedam IK. Upper airway 3d Changes of patients with cleft lip and palate after orthognathic surgery. *Cleft Palate Craniofac J*. 2019;56:314–320.
18. Dos Inocentes RJM, Marzano-Rodrigues MN, de Espíndola GG, et al. Adults with unilateral cleft lip and palate present reduced internal nasal volumes: Findings of a three-dimensional morphometric assessment in cone-beam computed tomography scans. *J Craniofac Surg*. 2021;32:e15, 374 9.
19. Yeom SH, Na JS, Jung HD, Cho HJ, Choi YJ, Lee JS. Computational analysis of airflow dynamics for predicting collapsible sites in the upper airways: machine learning approach. *J Appl Physiol*. 2019;127:959–973, 1985.
20. Banabilh SM, Suzina AH, Mohamad H, Dinsuhaimi S, Samsudin AR, Singh GD. Assessment of 3-D nasal airway morphology in Southeast Asian adults with obstructive sleep apnea using acoustic rhinometry. *Clin Oral Investig*. 2010;14:491–498.
21. Demirbas D, Cingi C, Cakli H, Kaya E. Use of rhinomanometry in common rhinologic disorders. *Expet Rev Med Dev*. 2011;8:769–777.
22. Genta PR, Sands SA, Butler JP, et al. Airflow shape is associated with the pharyngeal structure causing OSA. *Chest*. 2017;152:537–546.
23. Iwasaki T, Yoon A, Guilleminault C, Yamasaki Y, Liu SY. How does distraction osteogenesis maxillary expansion (DOME) reduce severity of obstructive sleep apnea? *Sleep Breath*. 2020;24:287–296.
24. Cherobin GB, Voegels RL, Gebrim EMMS, Garcia GJM. Sensitivity of nasal airflow variables computed via computational fluid dynamics to the computed tomography segmentation threshold. *PLoS One*. 2018;13, e0207178, 94.
25. Cherobin GB, Voegels RL, Pinna FR, Gebrim EMMS, Bailey RS, Garcia GJM. Rhinomanometry versus computational fluid dynamics: Correlated, but different techniques. *Am J Rhinol Allergy*. 2021;35:245–255.
26. Sullivan CD, Garcia GJ, Frank-Ito DO, Kimbell JS, Rhee JS. Perception of better nasal patency correlates with increased mucosal cooling after surgery for nasal obstruction. *Otolaryngol Head Neck Surg*. 2014;150:139–147.
27. Radulesco T, Meister L, Bouchet G, et al. Functional relevance of computational fluid dynamics in the field of nasal obstruction: A literature review. *Clin Otolaryngol*. 2019;44:801–809.
28. Yushkevich PA, Piven J, Hazlett HC, et al. User-guided 3D active contour segmentation of anatomical structures: significantly improved efficiency and reliability. *Neuroimage*. 2006;31:1116–1128.
29. Frank-Ito DO, Wofford M, Schroeter JD, Kimbell JS. Influence of mesh density on airflow and particle deposition in sinonasal airway modeling. *J Aerosol Med Pulm Drug Deliv*. 2016;29:46–56.
30. Gili JA, Poletta FA, Giménez LG, et al. Descriptive analysis of high birth prevalence rate geographical clusters of congenital anomalies in South America. *Birth Defects Res A Clin Mol Teratol*. 2016 Apr;106(4):257–266.
31. Tan J, Huang J, Yang J, et al. Numerical simulation for the upper airway flow characteristics of Chinese patients with OSAHS using CFD models. *Eur Arch Oto-Rhino-Laryngol*. 2013;270:1035–1043.
32. Yanagisawa-Minami A, Sugiyama T, Iwasaki T, Yamasaki Y. Primary site identification in children with obstructive sleep apnea by computational fluid dynamics analysis of the upper airway. *J Clin Sleep Med*. 2020;16:431–439.
33. Faizal WM, Ghazali NNN, Khor CY, et al. Computational fluid dynamics modelling of human upper airway: A review. *Comput Methods Programs Biomed*. 2020;196:105627–105649.
34. Xia G, Tawhai MH, Hoffman EA, Lin CL. Airway wall stiffening increases peak wall shear stress: a fluid-structure interaction study in rigid and compliant airways. *Ann Biomed Eng*. 2010;38:1836–1853.
35. Elcner J, Lizal F, Jedelsky J, Jicha M, Chovancova M. Numerical investigation of inspiratory airflow in a realistic model of the human tracheobronchial airways and a comparison with experimental results. *Biomech Model Mechanobiol*. 2016;15:447–469.
36. Liu X, Yan W, Liu Y, Choy YS, Wei Y. Numerical investigation of flow characteristics in the obstructed realistic human upper airway. *Comput Math Methods Med*. 2016;2016:3181654–3181655.
37. Kowalczyk DM, Hardy ET, Lewis AF. Airway evaluation in obstructive sleep apnea. *Oper Tech Otolaryngol - Head Neck Surg*. 2015;26:59–65.
38. Brouns M, Jayaraju ST, Lacor C, et al. Tracheal stenosis: a flow dynamics study. *J Appl Physiol*. 2007;102:1178–1184, 1985.
39. Phuong NL, Quang TV, Khoa ND, Kim JW, Ito K. CFD analysis of the flow structure in a monkey upper airway validated by PIV experiments. *Respir Physiol Neurobiol*. 2020;271:103304–103317.
40. Mylavarapu G, Murugappan S, Mihaescu M, Kalra M, Khosla S, Gutmark E. Validation of computational fluid dynamics methodology used for human upper airway flow simulations. *J Biomech*. 2009;42:1553–1559.
41. Lambeth C, Wang Z, Kairaitis K, Moshfegh A, Jabbarzadeh A, Amis TC. Modelling mucosal surface roughness in the human velopharynx: a computational fluid dynamics study of healthy and obstructive sleep apnea airways. *J Appl Physiol*. 2018;125:1821–1831, 1985.
42. Xu X, Wu J, Weng W, Fu M. Investigation of inhalation and exhalation flow pattern in a realistic human upper airway model by PIV experiments and CFD simulations. *Biomech Model Mechanobiol*. 2020;19:1679–1695.
43. Ma B, Lutchen KR. CFD simulation of aerosol deposition in an anatomically based human large-medium airway model. *Ann Biomed Eng*. 2009;37:271–285.
44. Allen GM, Shortall BP, Gemci T, Corcoran TE, Chigier NA. Computational simulations of airflow in an in vitro model of the pediatric upper airways. ASME *J Biomech Eng*. 2004;126:604–613.